

Analytical description of Ogston-regime biomolecule separation using nanofilters and nanopores

Zi Rui Li,^{1,*}† Gui Rong Liu,^{1,2} Jongyoon Han,^{3,4,*}‡ Yuan Cheng,^{2,5} Yu Zong Chen,^{1,6} Jian-Sheng Wang,^{1,7} and Nicolas G. Hadjiconstantinou⁸

¹The Singapore-MIT Alliance, EA-04-10, 4 Engineering Drive 3, Singapore 117576, Singapore

²Center for ACES, Department of Mechanical Engineering, National University of Singapore, Singapore 117576, Singapore

³Department of Electrical Engineering and Computer Science, Massachusetts Institute of Technology, Cambridge, Massachusetts 02139, USA

⁴Department of Biological Engineering, Massachusetts Institute of Technology, Cambridge, Massachusetts 02139, USA

⁵Institute of High Performance Computing, Singapore 138632, Singapore

⁶Department of Pharmacy, National University of Singapore, Singapore 117543, Singapore

⁷Department of Physics, National University of Singapore, Singapore 117542, Singapore

⁸Mechanical Engineering Department, Massachusetts Institute of Technology, Cambridge, Massachusetts 02139, USA

(Received 10 June 2009; published 8 October 2009)

We present a theoretical model describing Ogston (pore size comparable to or larger than the characteristic molecular dimension) sieving of rigid isotropic and anisotropic biomolecules in nanofluidic molecular filter arrays comprising of alternating deep and shallow regions. Starting from a quasi-one-dimensional drift-diffusion description, which captures the interplay between the driving electric force, entropic barrier and molecular diffusion, we derive explicit analytical results for the effective mobility and trapping time. Our results elucidate the effects of field strength, device geometry and entropic barrier height, providing a robust tool for the design and optimization of nanofilter/nanopore systems. Specifically, we show that Ogston sieving becomes negligible when the length of shallow region becomes sufficiently small, mainly due to efficient diffusional transport through the short shallow region. Our theoretical results are in line with experimental observations and provide important design insight for nanofluidic systems.

DOI: [10.1103/PhysRevE.80.041911](https://doi.org/10.1103/PhysRevE.80.041911)

PACS number(s): 87.15.Tt

I. INTRODUCTION

Understanding the physics of molecular sieving and filtration processes in porous materials, nanofilters or nanopores is of great importance in many areas of science and engineering [1–3]. The advent of micro- and nanofabrication has enabled a number of exciting new approaches in the area of nanofiltration; devices providing superior process control (e.g., precise and repeatable geometry, optical access, etc.) may now be built and optimized. One particular type of device consisting of a large number of deep wells connected by shallow slits [see Fig. 1(a)] has emerged as a promising gel-free sieving medium for separation of biomolecules including DNA, small proteins, etc. [4–7]. In addition to their use as a separation device, these systems are also ideal as experimental platforms for the study of the physics of nanoscale molecular sieving and filtration.

Experimental studies reveal that depending on the relative size of the molecule and slit (pore), different sieving mechanisms dominate [8]. Such studies have established that in the regime where the size of the biomolecule is smaller or comparable to the pore size, smaller molecules travel faster than bigger ones; this regime is known as Ogston sieving [8]. On the other hand, in the regime where the size of polyelectrolytes is much greater than the size of the pore, longer

molecules migrate faster than shorter ones [5,7]; the trapping mechanism in this regime is known as entropic trapping.

So far, a considerable number of theoretical and simulation studies of the transport dynamics in such systems have appeared [9–21]. Although these studies take a variety of points of view, most of simulation approaches use coarse-grained mesoscopic models to study the transport of long,

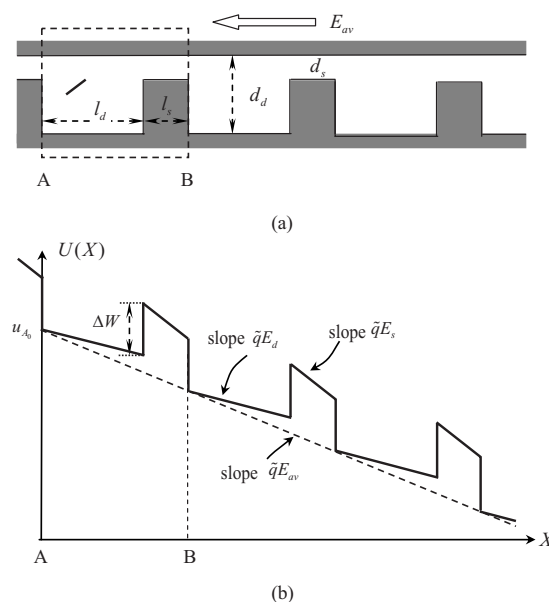


FIG. 1. (a) The nanofilter array consisting of alternative deep wells and shallow regions. (b) The potential-energy profile of a charged molecule along the nanofilter channel.

*Author to whom correspondence should be addressed.

†FAX: (+65)67791459; smalzr@nus.edu.sg

‡FAX: (+1)617-258-5846; jyhan@mit.edu

flexible molecules. Accurate description of such systems requires characterization of the polymer chain geometry and flexibility, the geometry of the filter or the pore, the presence of a nonuniform electric field, excluded volume effects [11], pore physical properties [13,14], electro-osmotic flow [15,18], and even the probability of hairpin formation as an initiator of polymer translocation [20,21]. Although some of this previous work provides key insights into the physical mechanisms and reproduces some experimental results qualitatively, the development of closed-form theoretical descriptions of the experimentally observed behavior remains very challenging and largely elusive.

In the Ogston sieving regime in particular, it is well known that the sieving effect is primarily caused by the steric hindrance at the pore entrance; as a result, the transport process was originally characterized by the free-volume model [22–24]. While this is strictly an equilibrium model, it is a good approximation for most molecular (gel and nanofilter) sieving situations. As an extension of the simple free-volume model, Fu *et al.* [7] recently incorporate the partitioning effect of orientational entropy [25] into a simplified Kramers rate theory to analyze their experimental results of molecular sieving in an array of regular periodic constrictions. Using this model, they were able to describe the field-dependent mobility of biomolecules in Ogston sieving, achieving a step forward from the near-equilibrium free-volume model. While their experimental results clearly demonstrated the existence of an Ogston sieving regime, a recent experiment with ultrashort (~ 10 nm) nanopores [26] reported a hard-core sieving behavior (exhibiting an abrupt cutoff in the transport of molecules exceeding some well-defined size) suggesting that nanopore/nanofilter systems exhibit significant sensitivity on structural parameters.

Besides the work of Fu *et al.* [7], other theoretical models of Ogston sieving based (mostly) on Kramers rate theory have been proposed [27–29]. Unfortunately, the physical setting assumed within the Kramers model is sufficiently different from that in nanofluidic filtration systems that *quantitative* predictions from the former are unreliable. For example, the Kramers model assumes parabolic potential landscape shapes (barrier/well), while the actual shape of the potential landscape in typical nanofiltration systems of interest as the one shown in Fig. 1(a), is approximately piecewise linear [see Fig. 1(b)]; additionally, the field-induced aggregation of molecules near the interfaces between the well and the barrier enhances the escape of molecules from the trap and speeds up the molecular transport; moreover, this aggregation of molecules induces a diffusive flux that differs from that in the Kramers model and may have a significant effect under certain conditions, especially when ultra short shallow regions are involved. Due to these differences, the Kramers model is expected to provide *quantitatively* reasonable results only under conditions of high barrier height and/or low field.

In order to gain more insight into the mechanism of Ogston sieving in nanofilter arrays, the present authors conducted simulation studies based on a continuum transport model [30] and macrotransport theory [31]. In these studies, the effects of channel size, slant angle, field strength, entropic barrier, and electroosmotic flow have been investigated qualitatively.

In the present paper, we derive an explicit analytical solution for the effective Ogston mobility of isotropic and anisotropic molecules in a nanofilter array using a drift-diffusion (Fokker-Planck) formulation within a quasi-one-dimensional (1D) geometry. Our results provide explicit relations quantifying (within the limits of applicability of the one-dimensional formulation) the effects of various design parameters, with no need for computationally expensive simulations. As we show in the discussion section, these results elucidate the contribution of several important transport mechanisms in the sieving processes, further contributing toward improved design and optimization of such devices. For example, unlike theories based on the Kramers model [6,28,29], the proposed model incorporates and *couples* information about the actual potential-energy landscape and diffusive transport in the entire device; as a result, as we show below, it not only captures, but is also able to quantify the effects of field-induced molecular aggregation at the deep-shallow—and depletion at the shallow-deep—transitions and its concomitant effect on transport.

Our formulation draws upon macrotransport theory [32]. A similar mathematical formulation albeit describing a different physical scenario—namely, the transport of spherical particles across a series of alternating immiscible fluid layers of different viscosity driven by a *constant* force—has appeared before [33]. In addition to the different physical context, the solution of [33] differs from ours in one important way: due to the constant force considered in [33], the ratio of drift velocity to diffusion coefficient (i.e., a measure of the Peclet number) is the same in the two fluid layers. On the other hand, in our formulation, due to a constant diffusion coefficient and variable force, the ratio of drift velocity to diffusion coefficient varies between the shallow and deep regions of the nanochannel. In fact, the two solutions become equivalent only in the limit where the nanofilter narrow and deep regions have the same depth (that is of no interest here), corresponding to a case of immiscible fluid layers that have the same viscosity.

II. FORMULATION

Description of the electric-field driven migration of charged Brownian particles in the nanofilter array shown in Fig. 1(a) under an external field is challenging because of the nonuniform electric field, variable device cross section, and the effect of the orientational degrees of freedom of the anisotropic biomolecules of interest here. In this work, we derive analytical results for the effective mobility and the trapping time for transport of these molecules based on a simplified one-dimensional model using macrotransport theory, a rigorous scheme for describing molecular transport in periodic structures in the long-time limit. In our model, anisotropic biomolecules are modeled as charged Brownian particles in a potential field, with their orientational degrees of freedom accounted for by an entropy term. The two-dimensional electric field is replaced by a one-dimensional effective field, which is piecewise constant in the deep and shallow regions, respectively.

A. Problem statement

We consider the transport of small, charged, Brownian, anisotropic biomolecules in nanodevices of the type shown in Fig. 1, comprising a large number ($N \sim 10\,000$) of alternating deep wells (length l_d and depth d_d) and shallow regions (length l_s and depth d_s) and kept at a constant temperature T . We assume that the molecules of interest are sufficiently short or rigid for a rigid-molecule approximation to be reasonable. Such molecules are treated as rigid cylindrical rods, lengths of which are determined using the Kratky-Porod model [34,35].

Let $\mathbf{R}=(X, Y, Z)$ denote the position vector with respect to a fixed origin located at point A as shown in Fig. 1, with X denoting the axial channel direction, Y the channel depth direction and Z the width direction. Also, let $L=l_d+l_s$ be the repeat length, $\varepsilon=d_s/d_d$ ($0 \leq \varepsilon \leq 1$) represent the depth ratio and $\nu=l_s/l_d$ the length ratio between the shallow region and deep well of the nanofilter.

The device is subject to an electric field of ‘‘average’’ magnitude $E_{av}=\Delta\Phi/(NL)$, where $\Delta\Phi=\Phi(NL)-\Phi(0)$ is the electric potential difference applied across the device. The relative importance of diffusion and electric force is quantified by the (translational) Peclet number [36] given by

$$\text{Pe} = \alpha\Psi, \quad (1)$$

where

$$\alpha = \frac{\varepsilon}{\varepsilon + \nu} \left(\frac{d_d}{l_d} \right)^2, \quad (2)$$

is a nanochannel-specific constant, and

$$\Psi = -\tilde{q}E_{av}L/k_B T, \quad (3)$$

is the dimensionless energy drop over a unit of nanochannel ($\Psi > 0$). Here k_B is Boltzmann’s constant and \tilde{q} is the molecule effective charge discussed in detail in the next section (we assume $\tilde{q} < 0$ due to the fact the DNA molecules carry negative charges). As we discuss below, although our mathematical solution is valid for all Pe, our modeling assumptions require $\text{Pe} \ll 1$, although they remain reasonable up to $\text{Pe} \sim \mathcal{O}(1)$, this range of Pe includes the majority of applications of interest here. Also note that for typical device geometries

$\alpha \ll 1$, implying that $\text{Pe} \leq 1$ may be satisfied even for large values of Ψ ; for example, the nanofilter device primarily studied later ($d_s=55$ nm, $d_d=300$ nm, and $l_d=l_s=0.5$ μm) is characterized by $\alpha \approx 0.056$.

B. Effective charge

In our model, electric-field driven motion of biomolecules is characterized by an effective charge \tilde{q} . Such a description is necessary because in aqueous solutions the effective charge of a polyelectrolyte appears to be much lower than the net charge q carried by its elements in vacuum [37–39] due to significant screening from the counterion cloud surrounding the molecule. This aggregation of counterions is also responsible for the difference observed in experiments between the effective hydrodynamic friction coefficient for

diffusion ς_d and the friction coefficient for electric-driven motion ς_e [40,41]. This is because when the molecule is subjected to random thermal motion, most of the surrounding counterions move with it; on the other hand, when a polyelectrolyte is driven by an electrostatic field, the counterions surrounding it will move in the opposite direction.

The approach taken here is to choose the value of the effective charge such that diffusion and the electric-field-driven motions are unified with a common, *orientationally averaged*, friction coefficient ς , chosen here to be equal to the friction coefficient for diffusion, i.e., $\varsigma = \varsigma_d$. This choice is informed by experiments [42], which show that the diffusion coefficient

$$D_d = k_B T / \varsigma_d \quad (4)$$

remains unaltered in the presence of electric fields. To determine the value of the effective charge, we consider the drift speed of a molecule in aqueous solution subjected to an electrostatic field of strength \mathbf{E} , and require that the observed velocity, $\tilde{\mathbf{V}} = q\mathbf{E}/\varsigma_e$, be equal to the theoretical velocity using the unified friction coefficient, i.e., $\tilde{\mathbf{V}} = \tilde{q}\mathbf{E}/\varsigma$. This requirement implies that the effective charge of the polyelectrolyte is given by $\tilde{q} = q\varsigma/\varsigma_e$. Expressing the charge in terms of more experimentally accessible diffusion coefficient in Eq. (4) and electrophoretic mobility [43], $\mu_0 = |\tilde{\mathbf{V}}|/|\mathbf{E}|$, the effective charge acquires the form,

$$\tilde{q} = -k_B T \mu_0 / D_d. \quad (5)$$

C. Dynamics of biomolecule transport in periodic nanofilter arrays

The motion of a Brownian particle of mass m in a potential field is described by the Langevin equation [44],

$$m\ddot{\mathbf{R}} = -\nabla U(\mathbf{R}) - \varsigma\dot{\mathbf{R}}(t) + \boldsymbol{\xi}(t) \quad (6)$$

where $\mathbf{R} \equiv (X, Y, Z)$ denotes the location of the particle, $U(\mathbf{R})$ is the potential field, ∇ is the gradient operator, and $\dot{\mathbf{R}}$, $\ddot{\mathbf{R}}$ are the particle velocity and acceleration, respectively. The fluctuating force $\boldsymbol{\xi}(t)$ is a vector of Gaussian white-noise form, satisfying [44]

$$\langle \boldsymbol{\xi}(t) \rangle = \mathbf{0},$$

$$\langle \boldsymbol{\xi}(t) \boldsymbol{\xi}(t') \rangle = 2\varsigma k_B T \delta(t-t') \mathbf{I}. \quad (7)$$

where $\delta(t-t')$ is the Dirac delta function and \mathbf{I} denotes the identity tensor.

In the highly damped (strong friction) regime, where the inertial force in Eq. (6) is negligible compared with other forces, the stochastic dynamics of a particle can be described by the probability density function $P(\mathbf{R}, t)$ for the particle appearing at point \mathbf{R} in the device at time t , whose time evolution is governed by the Fokker-Planck equation [29],

$$\frac{\partial P(\mathbf{R}, t)}{\partial t} = -\nabla \cdot \mathbf{J}(\mathbf{R}, t), \quad (8)$$

with the probability flux $\mathbf{J}(\mathbf{R}, t)$ given by

$$\mathbf{J}(\mathbf{R}, t) = -\frac{k_B T}{\varsigma} \nabla P(\mathbf{R}, t) - \frac{1}{\varsigma} P(\mathbf{R}, t) \nabla U(\mathbf{R}). \quad (9)$$

The probability density function satisfies the normalization condition

$$\int \int \int_{\Gamma} P(\mathbf{R}, t) d^3 \mathbf{R} = 1, \quad (10)$$

where Γ represents the entire device volume.

Instead of solving the governing equations in the entire device volume, macrotransport theory [32] states that one can obtain the mean molecule velocity (and other transport quantities of interest) from a reduced intracellular description, involving the probability function $P_0^\infty(\mathbf{r})$, which describes the long-time particle probability density as a function of the *local coordinate* $\mathbf{r} \equiv (x, y, z)$, regardless of the specific repeat the molecule resides in [32,45]. Under this formulation, the reduced intracellular probability function $P_0^\infty(\mathbf{r})$ in the steady state is governed by

$$\nabla \cdot \mathbf{J}_0^\infty(\mathbf{r}) = 0 \quad (11)$$

where the probability flux $\mathbf{J}_0^\infty(\mathbf{r})$ is given by

$$\mathbf{J}_0^\infty(\mathbf{r}) = -\frac{k_B T}{\varsigma} \nabla P_0^\infty(\mathbf{r}) - \frac{1}{\varsigma} P_0^\infty(\mathbf{r}) \nabla U(\mathbf{r}). \quad (12)$$

The normalization condition now requires that

$$\int \int \int_{\Gamma_0} P_0^\infty(\mathbf{r}) d^3 \mathbf{r} = 1, \quad (13)$$

where Γ_0 represents the interstitial space of one unit of the nanofilter. In the present work the repeated unit was chosen as shown in Fig. 1(a) (identified by the dotted lines); note, however, that within macrotransport theory, this choice is arbitrary and mostly a matter of convenience [32].

Finally, $P_0^\infty(\mathbf{r})$ must be continuous at the boundaries with adjacent repeats of the nanofilter. By solution of Eqs. (11)–(13) with suitable boundary conditions, one can obtain the asymptotic (long-time) values of effective mobilities as described in Sec III below.

D. Orientational entropy

We proceed by modeling the biomolecules of interest as point particles by accounting for their orientational distributions through a local partition function $\kappa(\mathbf{r})$, where \mathbf{r} denotes the molecule center of mass. As defined here, $\kappa(\mathbf{r})$ quantifies the relative occurrence of mass centers at position \mathbf{r} compared with that in a bulk solution. In the quasiequilibrium state assumed here (where all the possible orientations of a rigid molecule are equally accessible) $\kappa(\mathbf{r})$ is equal to the local orientational partition function, which describes the ratio of number of permissible orientations to the total number of possible orientations [25]. Here a permissible orientation is one that involves no intersection between the molecule and the solid wall.

This *quasiequilibrium* approximation can be justified by the fact that the characteristic relaxation time associated with rotational diffusion is many orders of magnitude shorter than the average transit time for one device repeat. At room temperature, the rotational diffusion coefficient for 300bp DNA molecules is estimated to be of the order of $D_r \sim 10^4 \text{ rad}^2/\text{s}$ [46]. The corresponding relaxation time $t_r = 1/D_r \sim 10^{-4} \text{ s}$, is thus much smaller than the average residence time in each repeat ($\sim 0.1 \text{ s}$) [30]. Moreover, for the small molecules and low-to-moderate electric fields of interest here, the effect of electric torque is small. This can be quantified by calculating the rotational Peclet number [36],

$$\text{Pe}_r = \beta \frac{1 - \varepsilon}{1 + \varepsilon} \Psi, \quad (14)$$

where β is the ratio of molecule length to L . For Ogston sieving in typical devices of interest, $\beta \ll 1$; as a result, the condition $\text{Pe}_r \ll 1$ is typically satisfied when $\text{Pe} \ll 1$.

Based on this formulation, the local partition may be expressed in terms of an orientational entropy,

$$S(\mathbf{r}) = k_B \ln \kappa(\mathbf{r}), \quad (15)$$

leading to a potential energy [see Eqs. (9) and (12)] of the form

$$U(\mathbf{r}) = \tilde{q} \Phi(\mathbf{r}) - k_B T \ln \kappa(\mathbf{r}), \quad (16)$$

where $\Phi(\mathbf{r})$ represents the potential value of the external electric field at point \mathbf{r} .

E. One-dimensional formulation

Since the net transport of DNA molecules takes place in the direction of the channel axis, under appropriate conditions, the degrees of freedom in the depth and width directions of the channel can be eliminated by proper projections. In particular, because the width of the channel is significantly larger than the maximum channel depth (d_d) and no external force is applied in the width (z) direction, we may assume that the distribution in the z direction is uniform. In addition, provided equilibrium in the y direction of the channel is maintained by translational diffusion (i.e., the translational diffusion is dominant over drift due to the electric force) the distribution in the y direction may be assumed to be in the quasiequilibrium state determined by the local partition function. In addition to translational diffusion, we also note that the convective flux induced by the nonuniform electric-field lines at the transition between the deep and shallow regions additionally contributes toward a quasiequilibrium probability distribution in the y direction. Below we describe how a one-dimensional model is constructed from the general three-dimensional description presented above.

1. Electric field

Assuming fully insulating walls and applying a resistance in series model (resistance is inversely proportional to the area of the channel), we obtain the following expressions for the field strengths in the deep and shallow regions:

$$E_d = \frac{\varepsilon(1 + \nu)}{\varepsilon + \nu} E_{av};$$

$$E_s = \frac{1 + \nu}{\varepsilon + \nu} E_{av}. \quad (17)$$

2. Partition coefficients

From our discussion above, we expect the partition function $\kappa(\mathbf{r})$ to be independent of y and z . Moreover, since the partition function is not a function of x in both the deep and shallow regions except close to the transition (assumed here to be very sharp), we can describe the restriction on particle orientational distributions using a uniform (averaged) partition function for the deep (K_d) and shallow (K_s) regions of the nanofilter, respectively. By this formulation, K_d and K_s quantify the probability of a molecule appearing in the deep and shallow region of channel, respectively, compared to that in the respective volume of free solution, i.e.,

$$K_d = \frac{\int \int \int_{\Gamma_d} \kappa(\mathbf{r}) d^3 \mathbf{r}}{\int \int \int_{\Gamma_d} d^3 \mathbf{r}};$$

$$K_s = \frac{\int \int \int_{\Gamma_s} \kappa(\mathbf{r}) d^3 \mathbf{r}}{\int \int \int_{\Gamma_s} d^3 \mathbf{r}}, \quad (18)$$

where Γ_d and Γ_s denote the volumetric spaces of the deep and shallow regions of the nanofilter, respectively. We thus arrive at an experimentally relevant constant, namely, the partition coefficient,

$$K = K_s / K_d, \quad (19)$$

which describes the ratio of equilibrium concentration of a biomolecule in the shallow and deep regions of the nanofilter. Partition coefficients can be readily incorporated within macrotransport theory; a recent example includes modeling Brownian particles in two immiscible fluids for vector chromatography applications [33,47].

Equilibrium at the boundaries of the deep and shallow regions requires that

$$P_0^\infty(l_{d+}, y, z) = KP_0^\infty(l_{d-}, y, z);$$

$$P_0^\infty(0_-, y, z) = KP_0^\infty(0_+, y, z). \quad (20)$$

Note that the second jump condition occurs at the unit-cell periodic boundary.

3. Probability field

We proceed by reducing the dimensionality of the probability field. We define the steady-state marginal intracellular probability function ($P_{x,0}^\infty$) by

$$P_{x,0}^\infty(x) = \int \int_{A(x)} P_0^\infty(x, y, z) dy dz, \quad (21)$$

where $A(x)$ denotes the cross section at point x along channel axis in the reduced unit cell. From our discussions above, $P_0^\infty(x, y, z)$ is independent of y and z [$P_0^\infty(x, y, z) \equiv P_0^\infty(x)$], which yields

$$P_{x,0}^\infty(x) = \begin{cases} wd_d P_0^\infty(x) & 0 < x < l_d \\ wd_s P_0^\infty(x) & l_d < x < L \end{cases}. \quad (22)$$

The normalization condition [Eq. (13)] becomes

$$\int_0^L P_{x,0}^\infty(x) dx = 1. \quad (23)$$

The boundary condition [Eq. (20)] takes the form

$$P_{x,0}^\infty(l_{d+}) = \varepsilon K P_{x,0}^\infty(l_{d-});$$

$$P_{x,0}^\infty(0_-) = \varepsilon K P_{x,0}^\infty(0_+) [P_{x,0}^\infty(L_-) = \varepsilon K P_{x,0}^\infty(L_+)] \quad (24)$$

The above relationships may be cast as an effective partition coefficient between the deep and shallow region of magnitude εK . These relationships also lead to a potential-energy barrier,

$$\Delta W = -k_B T \ln \varepsilon K \quad (25)$$

in the shallow region of 1D effective channel [see Fig. 1(b)]. Finally the expression of the 1D energy landscape (U_x), takes the form

$$U_x(x) = \begin{cases} \tilde{q} E_d x & 0 < x < l_d \\ -k_B T \ln \varepsilon K + \tilde{q} E_d l_d + \tilde{q} E_s (x - l_d) & l_d < x < L \end{cases}. \quad (26)$$

4. Conservation of probability

We complete the projection procedure by deriving the one-dimensional form of probability conservation [Eq. (11)]. Let

$$\mathbf{J}_0^\infty(\mathbf{r}) \equiv ([\mathbf{J}_0^\infty(\mathbf{r})]_x, [\mathbf{J}_0^\infty(\mathbf{r})]_y, [\mathbf{J}_0^\infty(\mathbf{r})]_z). \quad (27)$$

By integrating Eq. (11) over the volume of the cell between two arbitrary x locations and using the divergence theorem, as well as the assumption that $[\mathbf{J}_0^\infty(\mathbf{r})]_x$ is independent of y and z , we obtain

$$J_{x,0}^\infty(x) = \int \int_{A(x)} [\mathbf{J}_0^\infty(x)]_x dy dz = \text{const} = J_0, \quad (28)$$

$$J_{x,0}^\infty(x) = -\frac{k_B T}{s} \frac{dP_{x,0}^\infty(x)}{dx} - \frac{1}{s} P_{x,0}^\infty(x) \frac{dU_x(x)}{dx}. \quad (29)$$

Flux equations [Eqs. (28) and (29)] with the potential-energy landscape given by Eq. (26), subject to normalization [Eq. (23)] and boundary conditions [Eq. (24)] constitute the 1D macrotransport description of the molecular transport in the nanofilter array given in Fig. 1. Solution of these equations is described below.

III. SOLUTION FOR THE MOBILITY AND TRAPPING TIME

Since $J_{x,0}^\infty(x) = J_0$, multiplying both sides of Eq. (29) by $e^{U_x(x)/k_B T}$, and integrating the products over the unit cell of nanofilter [cf. Fig. 1(b)], the following expression is obtained:

$$J_0 = \frac{k_B T}{s} [P_{x,0}^\infty(0_+) e^{U_x(0_+)/k_B T} - P_{x,0}^\infty(L_+) e^{U_x(L_+)/k_B T}] \bigg/ \int_{0_+}^{L_+} e^{U_x(x)/k_B T} dx. \quad (30)$$

Substituting $U_x(x)$ from Eq. (26) into Eq. (30), and applying the boundary condition

$$P_{x,0}^\infty(0_+) = P_{x,0}^\infty(L_+) = p_0, \quad (31)$$

we obtain the following expression for J_0 :

$$J_0 = \frac{k_B T}{l_d s} \frac{p_0 \varepsilon K \Psi}{[1 - \lambda_d(1 - K)](\varepsilon + \nu)}, \quad (32)$$

where

$$\lambda_d = [1 - e^{-\varepsilon \Psi / (\varepsilon + \nu)}] / (1 - e^{-\Psi}). \quad (33)$$

Substituting J_0 from Eq. (32) into Eq. (29), we obtain

$$P_{x,0}^\infty(x) = \begin{cases} \frac{K(1 - e^{-\Psi}) + [1 - e^{-\nu \Psi / (\varepsilon + \nu)}] e^{-\varepsilon \Psi (1-x/l_d) / (\varepsilon + \nu)}}{(1 - e^{-\Psi})[1 - \lambda_d(1 - K)]} p_0, & 0 < x < l_d \\ \frac{1 - \lambda_d(1 - K) e^{-\Psi(1+\nu-x/l_d) / (\varepsilon + \nu)}}{1 - \lambda_d(1 - K)} \varepsilon K p_0, & l_d < x < L. \end{cases} \quad (34)$$

It is straightforward to verify that this solution satisfies both jump conditions given in Eq. (24).

The average speed of the particles, $J_0 / P_{x,0}^\infty(x)$, is given by

$$V_{x,0}^\infty(x) = \begin{cases} \frac{k_B T}{l_d s} \frac{\varepsilon K}{(\varepsilon + \nu) \{K(1 - e^{-\Psi}) + (1 - K)[1 - e^{-\nu \Psi / (\varepsilon + \nu)}] e^{-\varepsilon \Psi (1-x/l_d) / (\varepsilon + \nu)}\}} \frac{(1 - e^{-\Psi}) \Psi}{\Psi} & 0 < x < l_d \\ \frac{k_B T}{l_d s} \frac{1}{(\varepsilon + \nu) \{1 - \lambda_d(1 - K) e^{-\Psi(1+\nu-x/l_d) / (\varepsilon + \nu)}\}} \frac{\Psi}{\Psi} & l_d < x < L. \end{cases} \quad (35)$$

The physical definition of the speed $V_{x,0}^\infty(x) = dx/dt$ allows one to obtain the transit time in the nanofilter by

$$\tau = \int_0^L [V_{x,0}^\infty(x)]^{-1} dx = (1 + \eta_t) \tau_{travel}, \quad (36)$$

where

$$\tau_{travel} = \frac{(\varepsilon + \nu)(1 + \varepsilon \nu)}{(1 + \nu)^2 \varepsilon} \frac{L}{\mu_0 E_{av}} \quad (37)$$

is the minimum travel time (in the absence of sieving) and the factor η_t is given by

$$\eta_t = \frac{(1 - K)(1 - \varepsilon^2 K)(\varepsilon + \nu)}{K(1 + \varepsilon \nu)} \frac{[1 - e^{-\varepsilon \Psi / (\varepsilon + \nu)}][1 - e^{-\nu \Psi / (\varepsilon + \nu)}]}{\varepsilon(1 - e^{-\Psi}) \Psi}. \quad (38)$$

The trapping time in the nanofilter caused by the entropy barrier can be written as

$$\tau_{trap} = \tau - \tau_{travel} = \eta_t \tau_{travel} \quad (39)$$

effective mobility in the nanofilter $\mu = \bar{V} / E_{av}$, which finally takes the form,

$$\mu = \frac{L}{\tau E_{av}} = \frac{1}{1 + \eta_t} \mu_{\max} \quad (40)$$

From the average drift velocity $\bar{V} = L / \tau$ one can get the where

TABLE I. Free solution transport parameters and partition coefficients of DNA molecules.

DNA size (bp)	μ_0 (10^{-4} cm ² V ⁻¹ s ⁻¹)	D_0 (10^{-7} cm ² s ⁻¹)	K
50	0.63	2.0	0.90
150	0.63	1.1	0.66
300	0.63	0.71	0.42

$$\mu_{\max} = \frac{(1 + \nu)^2 \varepsilon}{(\varepsilon + \nu)(1 + \varepsilon \nu)} \mu_0 \quad (41)$$

is the maximum sieving-free mobility (in the absence of sieving).

One can verify the accuracy of these expressions by verifying that they reproduce some established limiting results. For example, for the transport of point-sized particles ($K=1$) one obtains $\eta_t=0$, which yields $\mu=\mu_{\max}$ and $\tau_{\text{trap}}=0$ (no sieving). In the limit of severe sieving ($K \ll 1$) of molecules through small pores ($\varepsilon \ll 1$) under low electric fields ($\Psi \ll 1$), we obtain $\eta_t \approx 1/K$, which implies $\mu \approx K\mu_{\max}$, reproducing the so-called free-volume model [22–24].

IV. RESULTS AND DISCUSSION

In this section we present some results and predictions obtained from our model for transport of short, rigid, rodlike dsDNA molecules in the nanofilter array shown in Fig. 1 under varied electric fields. These results are compared to relevant theoretical models or experimental observations and serve to highlight the utility as well as the weaknesses of our model.

The geometric parameters of the nanofilter are $d_s=55$ nm, $d_d=300$ nm, and $l_d=l_s=0.5$ μm . We consider DNA molecules with contour lengths of 50bp, 150bp, and 300bp. The corresponding effective rod lengths are 14 nm, 45 nm, and 87 nm, respectively [34,35]. The effective charge \bar{q} is calculated using Eq. (5). In the present work, numerical values for the free-solution diffusion coefficient D_d are taken from the experimental results of Lukacs *et al.* [48]. Although the value of the free-solution mobility μ_0 can in principle be also determined from direct experimental measurements, a number of poorly characterized effects, such as electroosmotic flow and molecule-tagging additives, typically make this difficult. Fortunately, the similarity [49] between the electroosmotic flow profile and the electric field means that in most cases the former can be accounted for through a shift in free-solution mobility [30,31]. In the present work, μ_0 was inferred by comparison with the experimental data of Fu *et al.* [7].

The partition coefficients are calculated by discretizing the interstitial space of the unit nanofilter using square cells of size 1 nm, whereby the local orientational partition function $[\kappa(\mathbf{r})]$ is calculated at the center of each cell by enumerating the possible orientations of a rod whose center of mass is located at \mathbf{r} . Partition coefficients (K) are then calculated using Eqs. (18) and (19).

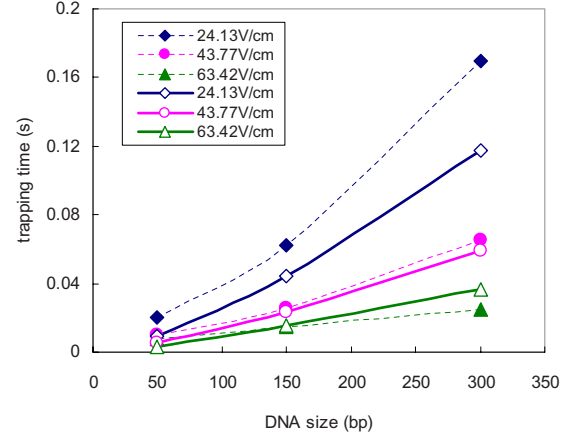


FIG. 2. (Color online) Comparison of analytical results (solid curves with hollow markers) and the experimental data (dotted curves with solid markers) for the trapping time [7].

Thus, in this formulation, a DNA molecule is characterized by three parameters, namely, \bar{q} , D_d , and K , the last of which is also dependent on the geometry of the nanofilter device. The parameters of different DNA molecules used in the subsequent calculations are listed in Table I.

Figure 2 shows the comparison of the trapping time as a function of molecule length and electric-field strength with the experimental data of Fu *et al.* [7]. The largest Peclet number associated with these data is 0.31 (associated rotational Peclet number is 0.34), placing most of the experimental data well within the validity range of our model, but also enabling us to test the validity of our model beyond its strict limits of applicability. The agreement with experiments is good, especially after considering that no particular attempt at optimizing the agreement was made and that the experimental results should differ somewhat from our predictions due to a number of “complicating” or poorly characterized

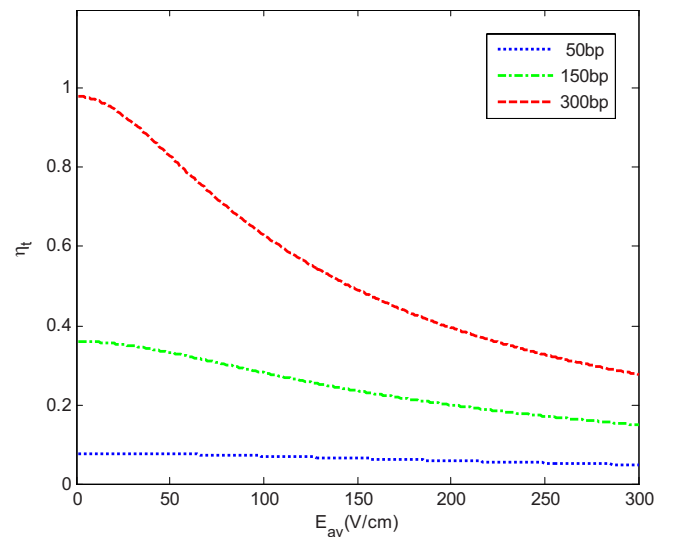


FIG. 3. (Color online) The field dependence of the trapping effect $\eta_t = \tau_{\text{trap}} / \tau_{\text{travel}}$ of dsDNA molecules in the nanofilter. Trapping effect is maximized at low electric fields, leading to better separation.

effects not included in our model, such as the exact geometry of the sieving structures (e.g., sloped walls, mildly variable well and shallow-region depths, etc.), the presence of complex electroosmotic flow, complex partitioning of the molecules in the Debye layer, flexibility of DNA molecules, etc. In the following sections we discuss our model predictions for the effect of various factors on the nanofilter performance.

A. Effect of the field strength

As a specific molecule with a given \bar{q} migrates in a nanofilter with specific values of L , ε and ν , Ψ is proportional to the electric field E_{av} . Figure 3 shows the dependence of the trapping delay on the electric-field strength for DNA molecules of length 50bp, 150bp, and 300bp. The trapping effect decreases swiftly with increasing field strength. More explicitly, noting that $\Psi \propto E_{av}$, from Eq. (38) it is easy to see that the field dependence of η_t changes from $\eta_t \sim E_{av}^0$ ($\tau_{trap} \sim E_{av}^{-1}$) at low field ($\Psi \ll 1$) to $\eta_t \sim E_{av}^{-1}$ ($\tau_{trap} \sim E_{av}^{-2}$) at high field [$\Psi \gg 1$, which for typical devices corresponds to $Pe > O(1)$]. Thus at sufficiently high electric field, $\eta_t \sim 0$, suggesting a negligible trapping effect, although it needs to be recalled that, as explained before, a number of our modeling assumptions may be invalid for $Pe \gg 1$. Despite this, the loss of trapping effect at high field has been observed both in experimental studies [6] and stochastic model simulations [36]. The work in [36] also identified a contribution that becomes important at high fields, namely, torque-assisted escape. According to our model, a high electric field results in significant molecule aggregation at the deep-shallow transition, leading to an increased escape rate. Therefore, low electric field is recommended for effective separation utilizing the difference in trapping time of biomolecules.

B. Effect of partition coefficient

Equations (38) and (39) indicate that the K dependence of trapping time takes the form $\tau_{trap} \sim (1-K)(1-\varepsilon^2 K)/K$. This relationship, valid for all K , includes contributions from the fraction of molecules entering the pore (K), the fraction of rejected molecules ($1-K$) and the diffusive flux in the narrow region ($1-\varepsilon^2 K$). This is in contrast to Kramers-type models, which predict $\tau_{trap} \sim 1/K$ (in agreement with our result only for $K \ll 1$).

Since longer molecules have smaller values of K , the above expression predicts that longer molecules travel slower, in agreement with experimental observations of the length dependence of mobilities of short DNA molecules [7]. This tendency is also in line with the scaling theory for linear translocation because no hairpin can be formed in short DNA rods and the translocation is always led by its ends [20].

Noting that K is dependent on both the molecular size and filter geometry, an ideal filter design should produce well separated values of $(1-K)(1-\varepsilon^2 K)/K$ for the molecules to be separated efficiently.

C. Effect of length of shallow region

The length of the shallow region (l_s), which has been neglected in most models based on Kramers theory, plays an

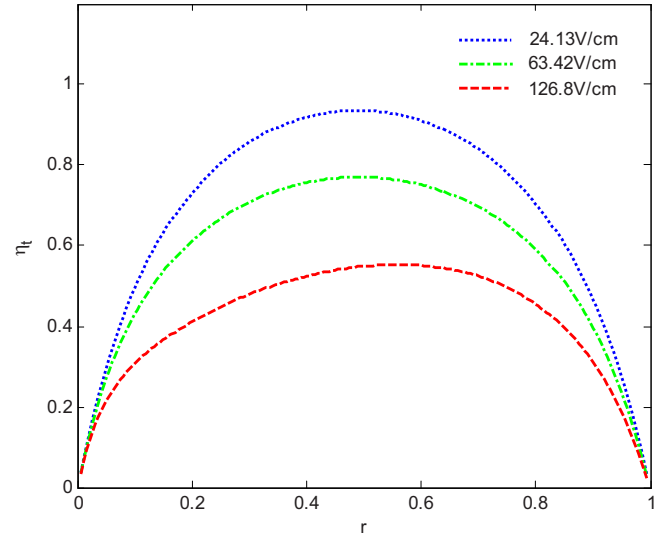


FIG. 4. (Color online) Dependence of trapping effect of 300bp dsDNA on $r=l_s/L$. In the low-field regime ($\Psi \ll 1$) maximum trapping occurs for $l_d=l_s$. The trapping time approaches 0 for very long or ultrashort shallow regions.

important role in hindered transport of molecules in nanofluidic systems. As an example, Fig. 4 shows the dependence of trapping effect as a function of l_s under varied field strengths. Specifically, the abscissa denotes the ratio of the shallow region in total nanofilter $r=l_s/L=\nu/(1+\nu)$. Thus $r \rightarrow 0$ represents an ultrashort shallow region; $r=0.5$ denotes equal length of deep and shallow regions ($l_d=l_s$), while $r \rightarrow 1$ corresponds to a very long shallow region. Under low electric fields ($\Psi \ll 1$), $\eta_t \approx \frac{(1-K)(1-\varepsilon^2 K)}{K} \frac{\nu}{(1+\varepsilon\nu)(\varepsilon+\nu)}$. Setting $d\eta_t/d\nu=0$ yields $\nu=1$, for all ε and K , suggesting that the trapping effect is maximized at the region close to $\nu=1$ in the low-field regime (see the solid curve representing an electric field of 24.13 V/cm in Fig. 4); thus $l_d=l_s$ is recommended for optimally utilizing the trapping effect to separate molecules.

An explicit expression for the value of ν that yields maximum trapping effect under higher electric fields is not available. However, from the dotted curve in Fig. 4, representing an electric field of 126.8 V/cm ($Pe \approx 0.63$), one may find that the maximum is shifted toward $\nu > 1$ ($l_s > l_d$), suggesting that, in this regime, one has to consider increasing the length of the shallow region to achieve better separation when higher electric field is adopted.

The results in Fig. 4 also show that for very short shallow region ($r \rightarrow 0$), the trapping effect becomes negligible ($\eta_t \rightarrow 0$). Such reduction of trapping effect and flux enhancement in ultrathin membranes (corresponding to a very small l_s in our system), has been observed in recent experiments [26]. Although this situation is not utilizing the entropic barrier, it may have potential in the area of size-exclusion ultrafiltration, because the flow of molecules smaller than the pore size is essentially not hindered. This indicates that ultrathin membranes are preferred for size-exclusion ultrafiltration, which can produce the highest possible production rate because all the molecules that can pass through are almost unhindered. Our model also predicts loss of the trapping effect in systems with a very long shallow region

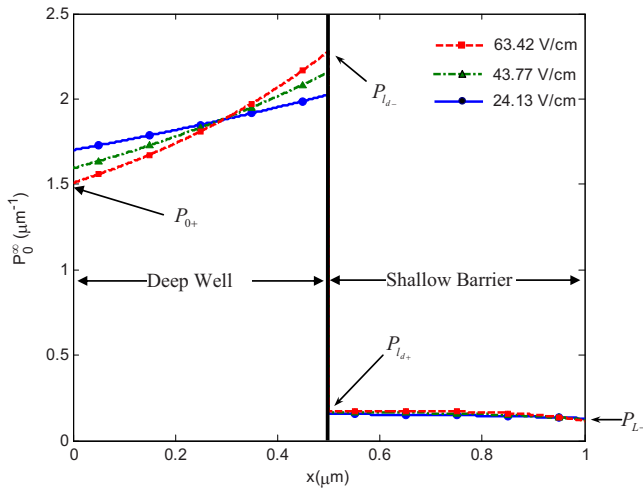


FIG. 5. (Color online) Reduced probability density profile of 300bp dsDNA molecules in a nanofilter with $K=0.42$ under different electric fields.

($\alpha \rightarrow 1, \nu \rightarrow \infty$). This setup is not expected to be frequently used in applications.

D. Role of nonuniform probability distribution and diffusion

Figure 5 shows the spatial distribution of reduced probability $P_{x,0}^{\infty}(x)$ of a 300bp dsDNA molecule ($K \approx 0.42$) under varied electric fields. Three electric-field strengths are considered, namely, 24.13, 43.77, and 63.42 V/cm; the corresponding Peclet numbers are 0.12, 0.22, and 0.31, respectively, while the corresponding rotational Peclet numbers are 0.13, 0.23, and 0.34, respectively. The jump in $P_{x,0}^{\infty}(x)$ at the interface between the deep and shallow region, namely, $P_{x,0}^{\infty}(l_{d+})/P_{x,0}^{\infty}(l_{d-}) = \varepsilon K = 0.077$, is a result of the potential-energy jump at the interface [see Eqs. (24) and (25) and the discussion of section 2.6.3]. Similar jumps can be seen at the cell edge (cf. Fig. 1) where, $P_{x,0}^{\infty}(0_-)/P_{x,0}^{\infty}(0_+) = \varepsilon K$ [or, equivalently, $P_{x,0}^{\infty}(L_-)/P_{x,0}^{\infty}(L_+) = \varepsilon K$].

Figure 5 provides a number of insights into the transport process, such as the effect of the entropy barrier at the deep-shallow region junction, the field-induced molecular aggregation in the same region, and the resulting impact on the migration dynamics. The entropy barrier hinders the drift of biomolecules, causing them to aggregate at the entrance to the narrow region. This aggregation process is balanced by diffusion, which acts toward creating a uniform distribution. A direct implication of this is that, in addition to free-resolution mobility, the overall electrophoretic mobility of molecules in the nanofilter is affected by their diffusivity.

Our results show that, compared to the residence time with no sieving $\tau_d^0 = l_d / \mu_0 E_d$, the molecule's average residence time in the well increases to $\tau_d = (1 + \eta_d) \tau_d^0$. The relative delay in the well, η_d , is given by

$$\eta_d = \frac{1 + \varepsilon \nu}{1 - \varepsilon^2 K} \eta_r. \quad (42)$$

On the other hand, the nonuniform particle distribution in the shallow region results in diffusive transport that decreases

the residence time from $\tau_s^0 = l_s / \mu_0 E_s$ to $\tau_s = (1 - \eta_s) \tau_s^0$, where

$$\eta_s = \frac{\varepsilon K}{\nu} \frac{1 + \varepsilon \nu}{1 - \varepsilon^2 K} \eta_r. \quad (43)$$

The total residence time in the nanofilter changes from the sieving-free value $\tau_{travel} = \tau_d^0 + \tau_s^0$ to $\tau = (1 + \eta_r) \tau_{travel}$.

V. CONCLUDING REMARKS

We have presented an analytical solution of a quasi-one-dimensional formulation of Ogston sieving of biomolecules in nanofilters utilizing an array of deep and shallow regions. Our model is based on a number of assumptions such as a uniform electric field in both the deep and shallow regions, and that the molecules of interest are sufficiently short or rigid for a rigid-molecule model to be valid. Moreover, we assume that the distribution of particles is uniform in the directions transverse to the direction of travel, that sufficient time exists for molecules to sample all possible rotational configurations at all the points in a nanofilter unit, and that torque-assisted escape effects [36] are negligible. As discussed above, the latter assumptions are expected to be valid for small molecules under low electric fields ($Pe \ll 1$), although we believe that they remain reasonable even for moderate electric fields ($Pe \leq 1$). We would like to emphasize, however, that even if these assumptions are not valid (e.g., for $Pe \gg 1$), our analytical results remain an exact solution of the one-dimensional problem formulated in Secs. II and III.

The analytical expressions for the electrophoretic mobility and the trapping time presented reproduce both qualitatively and to a good extent quantitatively the size and electric-field dependence of effective mobility of biomolecules in the Ogston sieving regime [7]. In fact, the agreement of our model's predictions with available experimental results is very encouraging considering that a number of "complicating" or poorly characterized effects are not included in our model, such as the exact geometry of the sieving structures (e.g., sloped walls, mildly variable well and shallow-region depth, etc.), complex partitioning of the molecules in the Debye layer, etc.

The closed-form expressions derived from our model provide insight into the physical mechanisms of the separation process absent in previous Kramers-type models. In particular, particle aggregation before the entrance to the shallow region and its effect on the particle distribution and trapping time is highlighted and quantitatively described. The theoretical framework proposed in this paper can also be applied to other similar problems, such as biomolecule transport through nanopores or anisotropic nanofilter arrays [50,51], to provide insight into molecular transport at the nanoscale.

The special case where field strengths in the well and the shallow regions are equal (i.e., the case corresponding to the formulation of [33]) can be obtained directly from our results by replacing K with $K' = d_s K / d_d$ and ε with $\varepsilon' = 1$. Our mobility results are also in agreement with those calculated by numerical evaluation of the integral definitions given in [52].

Our assumption of fast equilibration of the rotational degrees of freedom allows the use of orientationally averaged transport coefficients (drag, diffusion coefficient). In general,

one may expect different average transport coefficients in the deep and shallow regions as a result of the different states available to the molecules in these two regions [30]. This phenomenon can be included in our formulation by a suitable redefinition of K .

The formulation derived in this paper can be applied to other charged particles traveling in nanofilter arrays, provided they can be treated as rigid bodies (isotropic or anisotropic). The resulting model requires knowledge of the particles' free-solution mobility, free-solution diffusivity and partition coefficients.

Future work will focus on developing explicit results for the effective dispersion in such nanofiltration systems. We expect the analytical solution to be complex, but reduce to the integral form given in [52] under the special case of constant field, and the explicit solution in [33] when, in ad-

dition to constant field, the friction coefficients of both immiscible fluid layers are identical.

Future work will also concentrate on extending the formulation presented here to longer molecules. This can be achieved using partition coefficients calculated from worm-like chain formulations [53]. We expect the results of such calculations to be acceptable for qualitative purposes in the transition between Ogston and entropic regimes. However, such a model will not be applicable in the entropic trapping regime.

ACKNOWLEDGMENTS

This work was funded by Singapore-MIT Alliance (SMA)-II, Computational Engineering (CE) program. The authors express their thanks to N. M. Kocherginsky for critically commenting on the manuscript.

-
- [1] J. L. Viovy, *Rev. Mod. Phys.* **72**, 813 (2000).
 [2] R. B. Schoch, J. Han, and P. Renaud, *Rev. Mod. Phys.* **80**, 839 (2008).
 [3] J. Fu, P. Mao, and J. Han, *Trends Biotechnol.* **26**, 311 (2008).
 [4] J. Han, S. W. Turner, and H. G. Craighead, *Phys. Rev. Lett.* **83**, 1688 (1999).
 [5] J. Han and H. G. Craighead, *Science* **288**, 1026 (2000).
 [6] J. Fu, P. Mao, and J. Han, *Appl. Phys. Lett.* **87**, 263902 (2005).
 [7] J. Fu, J. Yoo, and J. Han, *Phys. Rev. Lett.* **97**, 018103 (2006).
 [8] J. Han, J. Fu, and R. B. Schoch, *Lab Chip* **8**, 23 (2008).
 [9] M. Muthukumar, *Phys. Rev. Lett.* **86**, 3188 (2001).
 [10] M. Muthukumar, *J. Chem. Phys.* **111**, 10371 (1999).
 [11] C. Y. Kong and M. Muthukumar, *J. Chem. Phys.* **120**, 3460 (2004).
 [12] C. T. A. Wong and M. Muthukumar, *J. Chem. Phys.* **128**, 154903 (2008).
 [13] C. Y. Kong and M. Muthukumar, *Electrophoresis* **23**, 2697 (2002).
 [14] M. Muthukumar and C. Y. Kong, *Proc. Natl. Acad. Sci. U.S.A.* **103**, 5273 (2006).
 [15] C. T. A. Wong and M. Muthukumar, *J. Chem. Phys.* **126**, 164903 (2007).
 [16] M. Streek, F. Schmid, T. T. Duong, and A. Ros, *J. Biotechnol.* **112**, 79 (2004).
 [17] K. L. Cheng, Y. J. Sheng, S. Jiang, and H. K. Tsao, *J. Chem. Phys.* **128**, 101101 (2008).
 [18] D. Duong-Hong, J.-S. Wang, G. R. Liu, Y. Z. Chen, J. Han, and N. G. Hadjiconstantinou, *Microfluid. Nanofluid.* **4**, 219 (2008).
 [19] T. P. Lodge and M. Muthukumar, *J. Phys. Chem.* **100**, 13275 (1996).
 [20] C. Forrey and M. Muthukumar, *J. Chem. Phys.* **127**, 015102 (2007).
 [21] C. T. A. Wong and M. Muthukumar, *Biophys. J.* **95**, 3619 (2008).
 [22] A. G. Ogston, *Trans. Faraday Soc.* **54**, 1754 (1958).
 [23] C. J. O. R. Morris, in *Protides of the Biological Fluids*, edited by H. Peeters (Elsevier, Amsterdam, 1966), Vol. 14, pp. 543.
 [24] D. Rodbard and A. Chrambach, *Proc. Natl. Acad. Sci. U.S.A.* **65**, 970 (1970).
 [25] J. C. Giddings, E. Kucera, C. P. Russell, and M. N. Myers, *J. Phys. Chem.* **72**, 4397 (1968).
 [26] C. C. Striemer, T. R. Gaborski, J. L. McGrath, and P. M. Fauchet, *Nature (London)* **445**, 749 (2007).
 [27] P. Hänggi, P. Talkner, and M. Borkovec, *Rev. Mod. Phys.* **62**, 251 (1990).
 [28] W. H. Stockmayer, in *Molecular Fluids*, edited by R. Balian and G. Weill (Gordon & Breach, London, 1976), pp. 107–149.
 [29] A. Ajdari and J. Prost, *Proc. Natl. Acad. Sci. U.S.A.* **88**, 4468 (1991).
 [30] Z. R. Li, G. R. Liu, Y. Z. Chen, J.-S. Wang, H. Bow, Y. Cheng, and J. Han, *Electrophoresis* **29**, 329 (2008).
 [31] Z. R. Li, G. R. Liu, J. Han, Y. Z. Chen, J.-S. Wang, and N. G. Hadjiconstantinou, *Anal. Bioanal. Chem.* **394**, 427 (2009).
 [32] H. Brenner, and D. A. Edwards, *Macrotransport Process* (Butterworth-Heinemann, Boston, MA, 1993).
 [33] K. D. Dorfman and H. Brenner, *J. Colloid Interface Sci.* **238**, 390 (2001).
 [34] O. Kratky and G. Porod, *Rec. Trav. Chim. Pays-Bas* **68**, 1106 (1949).
 [35] J. F. Marko and E. D. Siggia, *Macromolecules* **28**, 8759 (1995).
 [36] N. Laachi, C. Delet, C. Matson, and K. D. Dorfman, *Phys. Rev. Lett.* **98**, 098106 (2007).
 [37] M. Beer, M. Schmidt, and M. Muthukumar, *Macromolecules* **30**, 8375 (1997).
 [38] M. Muthukumar, *J. Chem. Phys.* **120**, 9343 (2004).
 [39] S. Liu, and M. Muthukumar, *J. Chem. Phys.* **116**, 9975 (2002).
 [40] J.-F. Mercier and G. W. Slater, *Electrophoresis* **27**, 1453 (2006).
 [41] E. Stellwagen, Y. J. Lu, and N. C. Stellwagen, *Biochemistry* **42**, 11745 (2003).
 [42] A. E. Nkodo, J. M. Garnier, B. Tinland, H. Ren, C. Desruisseaux, L. C. McCormick, G. Drouin, and G. W. Slater, *Electrophoresis* **22**, 2424 (2001).

- [43] M. Muthukumar, *Electrophoresis* **17**, 1167 (1996).
- [44] C. W. Gardiner, *Handbook of Stochastic Methods* (Springer-Verlag, Berlin, Heidelberg, 1983).
- [45] E. Yariv and K. D. Dorfman, *Phys. Fluids* **19**, 037101 (2007).
- [46] M. M. Tirado, C. L. Martinez, and J. Garcia de la Torre, *J. Chem. Phys.* **81**, 2047 (1984).
- [47] A. Leo, C. Hansch, and D. Elkins, *Chem. Rev.* **71**, 525 (1971).
- [48] G. L. Lukacs, P. Haggie, O. Seksek, D. Lechardeur, N. Freedman, and A. S. Verkman, *J. Biol. Chem.* **275**, 1625 (2000).
- [49] E. B. Cummings, S. K. Griffiths, R. H. Nilson, and P. H. Paul, *Anal. Chem.* **72**, 2526 (2000).
- [50] C. Dekker, *Nat. Nanotechnol.* **2**, 209 (2007).
- [51] J. Fu, R. B. Schoch, A. L. Stevens, S. R. Tannenbaum, and J. Han, *Nat. Nanotechnol.* **2**, 121 (2007).
- [52] N. Laachi, M. Kenward, E. Yariv, and K. D. Dorfman, *EPL* **80**, 50009 (2007).
- [53] G. N. Fayad and N. G. Hadjiconstantinou, *Microfluid. Nanofluid.* (to be published).